Physics of the Solid State, Vol. 46, No. 6, 2004, pp. 1055–1060. Translated from Fizika Tverdogo Tela, Vol. 46, No. 6, 2004, pp. 1025–1030.
Original Russian Text Copyright © 2004 by Krivtsov.

DEFECTS, DISLOCATIONS, AND PHYSICS OF STRENGTH

Molecular Dynamics Simulation of Plastic Effects upon Spalling

A. M. Krivtsov

Institute for Problems in Mechanical Engineering, Russian Academy of Sciences, Vasil'evskiĭ Ostrov, Bol'shoĭ pr. 61, St. Petersburg, 199178 Russia

e-mail: krivtsov@AK5744.spb.edu

Received June 2, 2003; in final form, September 26, 2003

Abstract—The molecular dynamics method is applied to simulate spalling during the plane shock interaction between plates. The effect of lattice defects in a material on the propagation of a shock wave and the process of spalling is studied. The plastic effects are described using a model of imperfect particle packing with defects (vacancies). The model proposed can describe the separation of the shock-wave front into an elastic precursor and a plastic front and give velocity profiles for the free target surface close to the experimental profiles. © *2004 MAIK "Nauka/Interperiodica".*

1. INTRODUCTION

In the last decades, the molecular dynamics (MD) method has been widely used to simulate the deformation and fracture of solids [1–5]; the representation of a material as a set of interacting particles allows one to describe its mechanical properties at both the micro- and macrolevel [6, 7]. To construct computer models for high-strain-rate fracture of materials, it is convenient to use the results of full-scale spalling tests, in which extremely high loads are created in a material under the conditions of uniaxial deformation [8–10]. In most works dealing with the MD simulation of spalling, ideal single-crystal particle packing was studied [11–13]. However, the mechanical properties of materials are rather sensitive to structural defects [14, 15]. Moreover, in many processes where real materials exhibit plastic properties, single crystals behave elastically until fracture. Although plastic behavior manifests itself upon MD simulation of the propagation of shock waves in single crystals [16], it differs substantially from the plastic deformation of real materials. In particular, in full-scale tests, a shock wave is clearly divided into an elastic precursor and a plastic front, whereas this division is weak or even absent in ideal single crystals. To solve this problem and describe the phenomena mentioned above, we propose a model of a crystalline material with artificially introduced structural defects (vacancies).

2. SIMULATION PROCEDURE

The simulation procedure applied in this work is identical to that used in [13, 17] and is described in detail in [18]. The material is represented by a set of particles interacting through a pair potential $\Pi(r)$. The equations of particle motion have the form

$$m\ddot{\mathbf{r}}_k = \sum_{n=1}^{N} \frac{f(|\mathbf{r}_k - \mathbf{r}_n|)}{|\mathbf{r}_k - \mathbf{r}_n|}(\mathbf{r}_k - \mathbf{r}_n), \quad (1)$$

where $\mathbf{r}_k$ is the radius vector of the kth particle, m is the particle mass, N is the total number of particles, and $f(r) = -\Pi'(r)$ is the interparticle interaction force. Contrary to [13], dissipative forces do not act in this system. We use the following notation: a is the equilibrium distance between two particles, $f(a) \equiv 0$, C is the stiffness of the interatomic bond in equilibrium, and T_0 is the period of vibrations of the mass m under the action of a linear force with stiffness C:

$$C = \Pi''(a) \cong -f'(a), \quad T_0 = 2\pi\sqrt{m/C}. \quad (2)$$

We will use the quantities a and T_0 as microscopic distance and time scales.

For a particle of mass m that is in equilibrium in the potential field $\Pi(r)$ to be at infinity, its minimum velocity (dissociation velocity) must be equal to

$$v_d = \sqrt{2D/m}, \quad (3)$$

where $D = \Pi(a)$ is the binding energy. The velocity of propagation of long-wavelength waves in an infinite chain is determined by the formula

$$v_0 = \sqrt{a^2 C/m}. \quad (4)$$

In this work, we analyze a two-dimensional material. In the case where particles are packed to form an ideal tri-

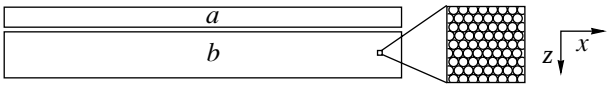

Fig. 1. Setup of the computer experiment: (*a*) impactor and (*b*) target.

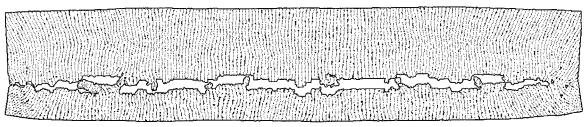

Fig. 2. Formation of a spalling crack.

angular (close-packed) crystal lattice, the velocity v_l of propagation of long longitudinal waves is

$$v_l = \sqrt{\frac{9}{8}} v_0 \approx 1.06 v_0. \quad (5)$$

We will illustrate these formulas for the case of the classical Lennard–Jones potential:

$$\Pi(r) = D\left[\left(\frac{a}{r}\right)^{12} - 2\left(\frac{a}{r}\right)^{6}\right], \quad (6)$$

where D and a are the binding energy and equilibrium interatomic distances introduced earlier, respectively. The corresponding interaction force $f(r) = -\Pi'(r)$ has the form

$$f(r) = \frac{12D}{a}\left[\left(\frac{a}{r}\right)^{13} - \left(\frac{a}{r}\right)^{7}\right]. \quad (7)$$

In the case of the Lennard–Jones potential, the stiffness C and binding energy D obey the relation $C = 72D/a^2$; therefore, the velocity of propagation of long waves and the dissociation velocity are connected by the simple relation $v_0 = 6v_d$. The Lennard–Jones potential is the simplest potential that allows one to take into account the general properties of interatomic interaction: repulsion of particles that approach each other, attraction of particles moving away from each other, and the absence of interaction at large distances between them. In this work, we study the principal possibility of describing the plastic effects upon spalling rather than simulate the behavior of a certain material; therefore, we will use only the Lennard–Jones potential. Our results can easily be extended to more complex potentials describing the properties of materials more exactly.

Calculation parameters

Parameter	Experiment		
	A	B	C
Approximate number of particles N	100000	500000	1000000
Impactor velocity v_{imp}	$1.05v_d$	v_d	$1.1v_d$
Particle-velocity deviation ΔV_0	$0.001v_d$	0	0
Vacancy concentration p, %	0	6	1
Cutoff radius a_{cut}	$2.1a$	$2.1a$	$2.1a$
Impactor (target) width w	$708a$	$1584a$	$2238a$
Impactor thickness h_1	$35a$	$78a$	$111a$
Target thickness h_2	$88a$	$196a$	$277a$
Number of particle layers N_z	142	319	450
Integration step Δt	$0.03T_0$	$0.03T_0$	$0.03T_0$
Calculation time $t_{\max}$	$3t_s$	$3t_s$	$3t_s$

3. SIMULATION OF SPALLING

Figure 1 shows the setup of the computer experiment. Particles form two rectangles lying in the *xz* plane; they simulate the sections of an impactor (*a*) and a target (*b*). The impactor and target consist of the same particles, whose interaction is described by Eq. (6). The particles are ordered to form a triangular lattice, which is identical for the impactor and target; the lattice is oriented so that one of its basis vectors is directed along the *x* axis. Free boundary conditions are used at all outer boundaries. The lattice parameter a_e in the initial configuration is chosen so as to ensure the absence of internal stresses at a cutoff radius of $2.1a$ [18].[1]

Initially, the target has a zero velocity and the impactor velocity is directed along the *z* axis toward the target. Moreover, at the initial instant of time, each particle in the impactor and target is given an additional random velocity that is chosen from a two-dimensional uniform random distribution with a given variance σ, defined as

$$\sigma = \frac{1}{n}\sum_{k=1}^{n}(V_k - \bar{V})^2, \quad \bar{V} = \frac{1}{n}\sum_{k=1}^{n} V_k. \quad (8)$$

Here, V_k is the projection of the velocity of the kth particle along the shock direction and k runs over the values specifying a certain set of particles that enters the total system of particles to be analyzed in the experiment. We also use the standard deviation of the particle velocities $\Delta V = \sqrt{\sigma}$.

The states of the impactor and target after simulation are shown in Fig. 2. A spalling crack formed in the target is clearly visible. However, the interface between the impactor and target is invisible because of the ideal coincidence of the contacting surfaces (matching of the crystal lattices in the impactor and target). The parameter values for this case are given in the table (experi-

[1] $a_e = 0.9917496a$.

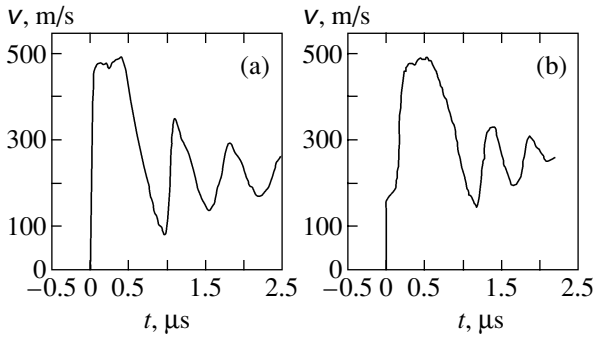

Fig. 3. Time dependence of the velocity of the free target surface for (a) single crystal (calculation) and (b) titanium alloy (experiment).

ment A). Computer experiments show that the minimum impactor velocity at which spalling begins is approximately equal to the dissociation velocity v_d; therefore, it is worthwhile to compare the velocities used in the calculation with this value (see table). The dimensions of the impactor and target in this computer experiment are such that $h_1/w \approx 1/20$ and $h_1/h_2 \approx 2/5$. The spalling time t_s can be estimated from the formula $t_s = (h_1 + h_2)/v_l$, where h_1 and h_2 are the thicknesses of the impactor and target, respectively, and v_l is determined from Eq. (5). In this case, $t_s = 18.4T_0$. Of course, this estimation is very rough, since v_l is the velocity of longitudinal waves according to linear theory; i.e., this velocity corresponds to small-amplitude waves. According to nonlinear theory, the larger the amplitude of waves in a single crystal, the higher their velocity. However, in a crystalline material with defects, the wave velocity can be lower than v_l. Moreover, a wave has a certain extent in space, which can also introduce error in the spalling time. Nevertheless, it is convenient to use the time t_s as a time scale, since it has a clear physical meaning and can easily be determined. The quantity N_z in the table is equal to the total number of particle layers (in the impactor + target system) along the shock direction.

Figure 3a shows the simulated time dependence of the velocity of the free target surface. To measure the velocity of the free surface, we used two lower particle layers, more specifically, only the central part of these layers of width $w_0 = w - 2(h_1 + h_2)$, to eliminate edge effects. The dependence obtained was averaged over time to exclude high-frequency vibrations. For comparison, Fig. 3b shows an analogous experimental dependence obtained during a full-scale spalling test of a titanium alloy at an impactor velocity of 602 m/s [9]. The time and velocity scales in Fig. 3a are chosen according to the full-scale experiment. The shapes of the curves are seen to be similar: the main maximum corresponding to the instant at which the shock wave reaches the free surface and vibrations in the target are clearly defined in both dependences. However, there are substantial differences. First, the shapes of the shock-wave fronts are different. In the full-scale experiment, the shock front is clearly divided into an elastic precursor and the subsequent plastic front, whereas this division is absent in the simulation. In the latter case, only the elastic component of the front exists and the plastic front is virtually absent; this behavior is caused by the ideal (defect-free) structure of the model single crystal.

To simulate plastic deformation at the shock front, we consider a crystalline material with lattice defects. As the initial material, we choose the single crystal mentioned above. To produce an imperfect material, we randomly remove atoms from the initial material to achieve the required defect (vacancy) concentration, which is calculated as the percentage ratio of the num-

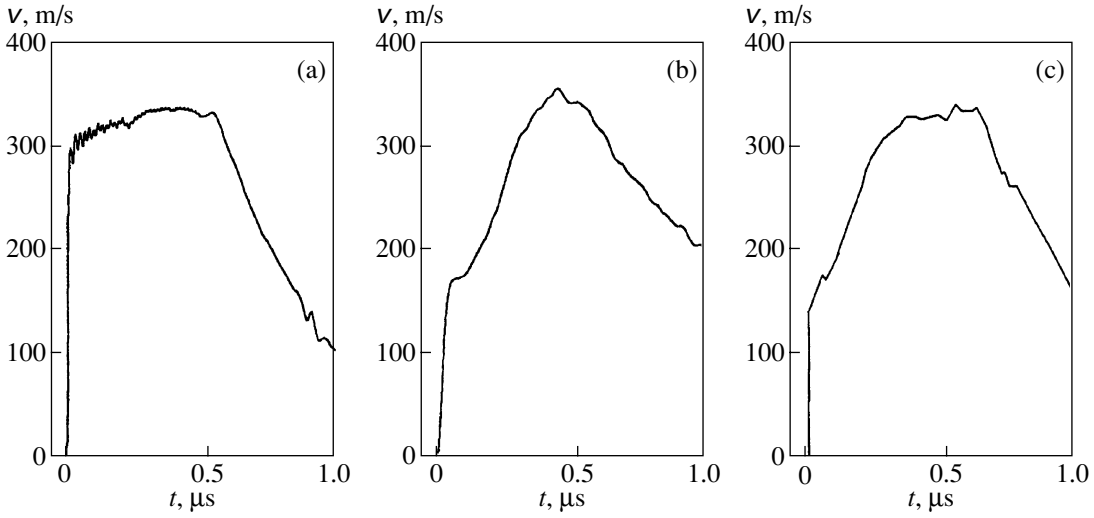

Fig. 4. Time dependence of the velocity of the free target surface for (a) a perfect single crystal (calculation), (b) a single crystal with defects (calculation), and (c) VT-20 titanium alloy (experiment).

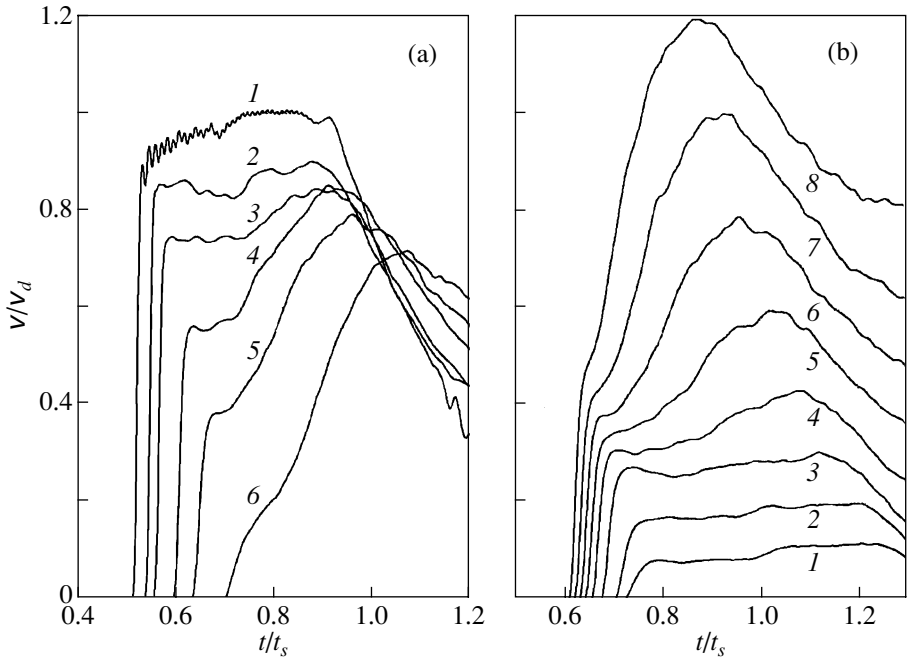

Fig. 5. Velocity profiles for the free target surface (simulation): (a) at $v_{imp} = v_d$ and a vacancy fraction of (*1*) 0, (*2*) 1, (*3*) 2, (*4*) 4, (*5*) 6, and (*6*) 9%; (b) at a vacancy fraction of 6% and v_{imp}/v_d equal to (*1*) 0.1, (*2*) 0.2, (*3*) 0.4, (*4*) 0.6, (*5*) 0.8, (*6*) 1.0, (*7*) 1.2, and (*8*) 1.4.

ber of removed atoms to the initial number of atoms. When a shock wave moves in such a material, vacancies initiate irreversible changes in its structure, which lead to plastic deformation of the medium.

The initial values of the parameters are given in the table (experiment B). The model contains $\sim 5 \times 10^5$ particles, with the ratios of the impactor and target dimensions remaining as before. Figures 4a and 4b show the time dependences of the velocity of the free surface when the shock wave reaches the surfaces of the perfect single crystal and the imperfect material (vacancy fraction 6%), respectively. For comparison, Fig. 4c shows the experimental curve recorded during a full-scale spalling test of a VT-20 titanium alloy at an impactor velocity of 365 m/s [9]. The time and velocity scales in Figs. 4a and 4b are chosen according to the experimental scales. In Fig. 4a, the shock-wave front is virtually vertical and carries only elastic deformation. In contrast, Figs. 4b and 4c demonstrate a pronounced elastic precursor followed by a plastic front.

The relation between the amplitudes of the elastic and plastic fronts depends on the defect concentration and the impactor velocity, which is illustrated in Figs. 5a and 5b. Figure 5a shows the velocity profiles of the target free surface simulated at the same parameters as those in Fig. 3b but at different defect concentrations. The time and velocity are measured in units of the calculated spalling time t_s and the dissociation velocity v_d. As the defect concentration increases, the elastic-precursor amplitude decreases significantly faster than the plastic-front amplitude, which leads to their distinct separation. Figure 5b shows the results of analogous simulations at the same defect concentration (6%) and various values of the impactor velocity v_{imp}. At low v_{imp} values ($v_{imp} \le 0.2v_d$), the shock-wave front contains only an elastic component. However, as the impactor velocity increases, a plastic component appears, which increases much faster than the elastic component with a further increase in v_{imp}.

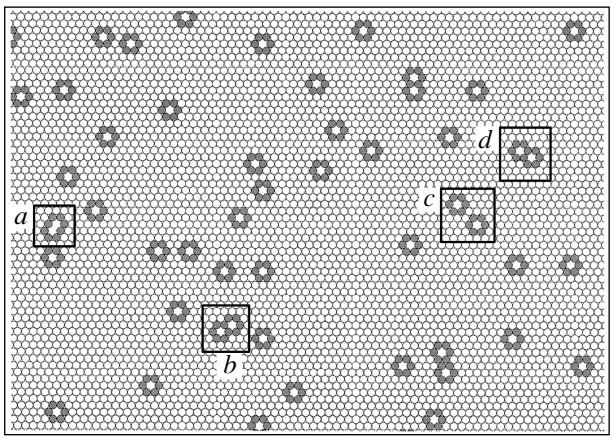

Fig. 6. Structure of the model material before passing a shock wave: (*a*) microvoid and (*b–d*) pairs of vacancies. The particles that have less than six neighbors at a distance of 1.1*a* are dark.

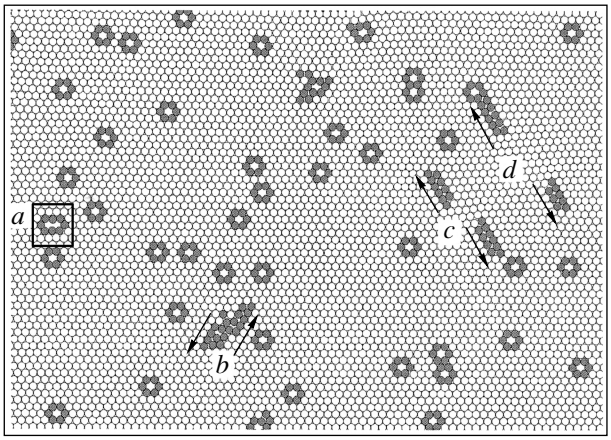

Fig. 7. Changes in the material structure upon passing a shock wave: (*a*) microvoid, (*b*) dislocation nucleation, and (*c*, *d*) decomposition of pairs of vacancies into dislocation pairs.

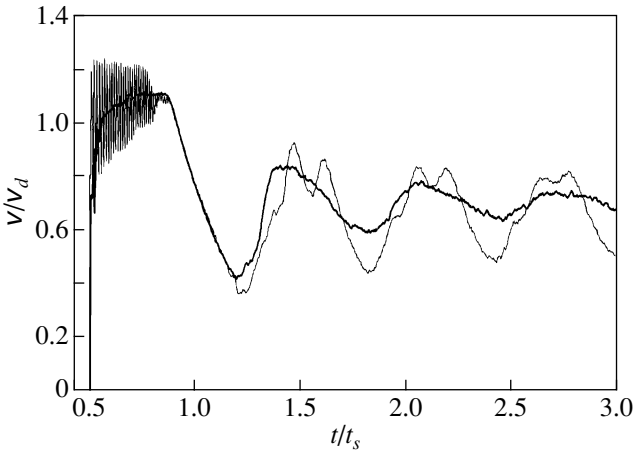

Fig. 8. Velocity profiles of the free target surface for the vacancy concentrations of 0 (thin line) and 0.1% (heavy line).

4. DISCUSSION OF THE RESULTS

To elucidate the behavior of defects at the shock-wave front, we consider an element of the model material before and after passing a shock wave (Figs. 6, 7). These pictures are obtained as a result of simulating spalling at the parameters given in the table (experiment C). The material element shown in Figs. 6 and 7 contains about 4800 particles, which is less than 0.5% of the total volume to be simulated. To study the behavior of defects, we analyzed the total volume; this element is shown only for illustration. In Figs. 6 and 7, the particles located near lattice defects are dark.[2] In the undeformed material (Fig. 6), the defects are vacancies. However, due to their random distribution, some of them are in immediate vicinity to each other and some vacancies combine to form microvoids (Fig. 6a). Let us choose several closely spaced vacancies (Figs. 6, vacancies *a*–*d*) and follow their evolution upon passing a shock wave (Fig. 7, vacancies *a*–*d*). Microvoid *a* in Fig. 7 is seen to change its orientation under the effect of the shock wave. As for the other chosen vacancy groups, they decompose into pairs of moving dislocations (Fig. 7, groups *c*, *d*; the arrows show the directions of dislocation motion). The shock front in Fig. 7 moves from the top down; therefore, different stages of the decomposition of the vacancy groups are visible in Fig. 7 (groups *b*–*d*): nucleation of dislocations (Fig. 7, group *b*) and their recession (Fig. 7, groups *c*, *d*). A comparison of single vacancies in Figs. 6 and 7 shows that a shock wave of the given intensity cannot cause their migration or transformation into dislocations. Thus, plasticity in the imperfect material under study occurs mainly via the decomposition of closely spaced vacancies to form dislocation-like defects, which causes shear strains at the shock front upon defect motion.

Note that even an insignificant number of defects results in a significant change in the velocity profile of the free surface. Figure 8 illustrates the results of simulating a perfect single crystal and a similar crystal where one atom per one thousand atoms is removed (the defect concentration is 0.1%). The impactor velocity is $v_{\text{imp}} = 1.1v_d$, and the values of the other parameters correspond to experiment B (see table). For illustration, the curves were not averaged over time. Therefore, the profile of the perfect single crystal demonstrates clearly visible high-frequency vibrations (induced by the discreteness of the MD representation) at the shock front. These vibrations virtually disappear in the material with defects. Moreover, the vibrations in the target strongly change in character and the rate of their damping increases significantly. At the low defect concentration used in the simulation, the elastic and plastic fronts cannot be separated. However, these fronts will likely be separated in this material as the crystal thickness along the shock direction increases.

5. CONCLUSIONS

Thus, when loaded with a shock wave, a single crystal consisting of particles that interact through the Lennard–Jones potential and containing a sufficient concentration of lattice defects demonstrates pronounced plastic effects, such as separation of the shock-wave front into elastic and plastic components. As a result, we could obtain time dependences of the velocity of the free target surface very close to the experimental curves, in particular, to the curves recorded upon spalling of titanium alloys.

[2] Specifically, the particles that have less than six neighbors at a distance of $1.1a$ are dark (in the ideal triangular lattice, the number of neighbors for each atom is equal to six).

ACKNOWLEDGMENTS

The author is grateful to Yu.I. Meshcheryakov for experimental data and useful discussions.

This work was supported by the Ministry of Education of the Russian Federation, project no. E02-4.0-33.

REFERENCES

1. B. L. Holian, Shock Waves **5** (3), 149 (1995).
2. A. I. Lobastov, V. E. Shudegov, and V. G. Chudinov, Zh. Tekh. Fiz. **70** (4), 123 (2000) [Tech. Phys. **45**, 501 (2000)].
3. V. A. Lagunov and A. B. Sinani, Fiz. Tverd. Tela (St. Petersburg) **43** (4), 644 (2001) [Phys. Solid State **43**, 670 (2001)].
4. F. F. Abraham, R. Walkup, H. Gao, M. Duchaineau, T. D. De La Rubia, and M. Seager, Proc. Natl. Acad. Sci. USA **99** (9), 5783 (2002).
5. A. M. Krivtsov, in *Problems in Mechanics of Deformed Solids* (S.-Peterb. Gos. Univ., St. Petersburg, 2002), pp. 173–178.
6. A. M. Krivtsov and N. F. Morozov, Dokl. Akad. Nauk **381** (3), 825 (2001) [Dokl. Phys. **46**, 825 (2001)].
7. A. M. Krivtsov and N. F. Morozov, Fiz. Tverd. Tela (St. Petersburg) **44** (12), 2158 (2002) [Phys. Solid State **44**, 2260 (2002)].
8. A. M. Rajendran and D. J. Grove, Int. J. Impact Eng. **18** (6), 611 (1996).
9. Yu. I. Mescheryakov, A. K. Divakov, and N. I. Zhigacheva, Shock Waves **10**, 43 (2000).
10. G. I. Kanel', S. V. Razorenov, and V. E. Fortov, in *Problems in Mechanics of Deformed Solids* (S.-Peterb. Gos. Univ., St. Petersburg, 2002), pp. 159–165.
11. N. J. Wagner, B. L. Holian, and A. F. Voter, Phys. Rev. A **45** (12), 8457 (1992).
12. W. C. Morrey and L. T. Wille, Comput. Mater. Sci. **10** (1–4), 432 (1998).
13. A. M. Krivtsov, Int. J. Impact Eng. **23** (1), 466 (1999).
14. S. P. Nikanorov and B. K. Kardashev, *Elasticity and Dislocation Inelasticity of Crystals* (Nauka, Moscow, 1985).
15. V. A. Lagunov and A. B. Sinani, Fiz. Tverd. Tela (St. Petersburg) **45** (3), 542 (2003) [Phys. Solid State **45**, 573 (2003)].
16. B. L. Holian and P. S. Lomdahl, Science **280** (5372), 2085 (1998).
17. A. M. Krivtsov and Y. I. Mescheryakov, Proc. SPIE **3687**, 205 (1999).
18. A. M. Krivtsov and N. V. Krivtsova, Dal'nevost. Mat. Zh. **3** (2), 254 (2002).

Translated by K. Shakhlevich